RSC Advances

ROYAL SOCIETY OF CHEMISTRY

www.rsc.org/advances

Table of Contents

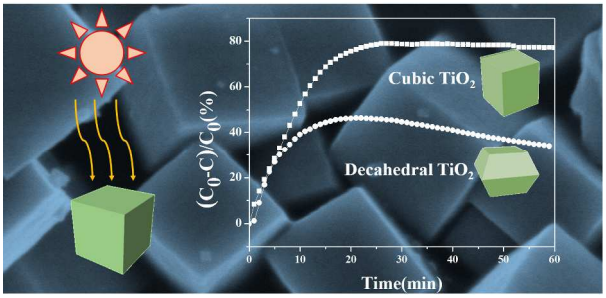

Uniform cubic anatase TiO_2 fully enclosed by high energy facets was prepared using green method for enhancing the photocatalytic activity.

Journal Name

RSCPublishing

ARTICLE

Uniform Anatase Single-Crystal Cubes with Highly Thermal Stability and Fully Enclosed by Active {010} and {001} Facets

Cite this: DOI: 10.1039/xoxxoooooox

Received ooth January 2012,
Accepted ooth January 2012

DOI: 10.1039/xoxxoooooox

www.rsc.org/

Meicheng Wen,[a, b,†] Peijue Liu,[a,†] Shuning Xiao,[a] Kohsuke Mori,[b,c] Yasutaka Kuwahara,[b,c] Hiromi Yamashita,[b,c,*] Hexing Li[a] and Dieqing Zhang[a,*]

In order to improve the photocatalytic activity of TiO_2, synthesis of well-faceted single crystal of anatase TiO_2 with a high percentage of reactive facets exposed has attracted much attention due to the fascinating surface atomic configuration. In this study, large anatase single crystal cubes with {001} and {010} facets exposed were prepared for the first time via a facile microwave-assisted method. The preparation involved an aqueous solution of titanium tetrachloride, ionic liquid (1-methyl-imidazolium tetrafluoroborate), and sodium dodecyl benzene sulfonate (SDBS) as titanium precursor, facet-directing agent, and surfactant, respectively. It is demonstrated that these single-crystalline TiO_2 crystals with cubic morphology showed the better photocatalytic performance than those decahedral anatase TiO_2 due to high density of unsaturated surface Ti_{5c} atoms on cubic TiO_2.

Introduction

Photocatalysis is regarded as one of the most promising technologies, which has played an important role in many application ranging from environmental purification to energy conversion.[1-7] Recently, titanium dioxide (TiO_2) is the most widely studied semiconductor in photocatalysis and energy conversion because it is readily available, chemically stable, inexpensive, and environmentally benign.[8-11] The physical and chemical properties as well as the photocatalytic reactivity of TiO_2 nanoparticles are very sensitive to their morphology and surface atomic configuration.[12] Intensive experimental and theoretical studies have been conducted on the reactivity of different facets of TiO_2 with unique morphology.[13-16] On the one hand, the surface physical/chemical properties such as adsorption, catalytic activity and selectivity is definitely affected by surface atomic arrangement and the degree of exposure of reactive crystal facets.[17] On the other hand, the particular morphology contributes to the fast electron transfer because of a surface hetero-junction can be formed between two different facets, thereby reducing photoelectron-hole recombination rate.[18-21] For example, Yu's group reported that the ratio of the exposed {001} and {101} facets significantly affects the photocatalytic activity of anatase toward reduction of CO_2.[22] Therefore, there is considerable interest in the controlled preparation of a specific crystal shaped TiO_2 with the largest exposure of high photoactive facets.

It is conventionally considered that a facet with a high percentage of unsaturated atom possesses a superior reactivity than that of with a low percentage of unsaturated Ti atom.[23,24] Basically, there are three fundamental low-index facets of anatase TiO_2 crystal: {101}, {001}, and {010}. In contrast to {101} facets with 50 % unsaturated Ti_{5c} atoms, {001} and {010} facets have 100 % unsaturated Ti_{5c} atoms. Furthermore, the surface energy of {001}, {010}, and {101} are known to be 0.90 J m^{-12}, 0.53 J m^{-12}, and 0.44 J m^{-12}, respectively.[25,26] Therefore, some researchers have suggested that {001} and {010} facets showed more reactive performance than {101} facets owing to having more unsaturated Ti_{5c} atoms and higher surface energy.[19,27] Fabrication of a high percentage of {010} facets and {001} facets anataste TiO_2 is therefore of great significance in optimizing the photocatalytic activity of anatase. However, single crystals anatase TiO_2 are thermodynamically inclined to fabricate truncated octahedron enclosed by {101} facets to minimize the total surface energy, resulting in the quickly diminishing the facets with high surface energy during the crystal growth process.[28] Recently, Yang's group[29] reported that surface Ti-F bonds can change the surface unsaturated Ti_{5c} atoms to Ti_{6c} and reduce the surface energy. The findings of this work open up new opportunities for maximizing the surface exposed {001} and {010} facets percentage through the modification of the surface atomic configuration. Up to now, a series of the synthetic routes have been developed to fabricate TiO_2 crystals with high energy facets exposed in the presence of extremely corrosive and toxic hydrofluoric acid.[30-33] However, those fabrication methods always result in low yield

single crystal TiO_2 with significant aggregation because the low pH value prevented titanium precursor from hydrolysis. In order to synthesize of highly dispersed single crystal TiO_2 with two different reactive facets exposed and with high yields, looking for a mild facet-directing agent and suitable surfactant is a prerequisite. This is still a big challenge for engineering of single crystal TiO_2 exclusively enclosed by {001} and {010} facets.

Inspired by the possibility of enhanced photocatalytic activity in shape controlled single crystal TiO_2 with a high percentage of reactive facets exposed and our previous reported works,[17,30] in this study, we have developed a synthetic strategy to the synthesis of highly dispersed single crystal TiO_2 cubes with predominant {001} and {010} facets. The single-crystal cubes were simply achieved by the microwave-assisted hydrothermal treatment of the aqueous solution of tetrachloride ($TiCl_4$) with ionic liquid as a facet-directing agent and sodium dodecyl benzene sulphonate (SDBS) as a surfactant. The fabrication process is quite simple and efficient because of free from toxic hydrofluoric acid. To the best of our knowledge, it is the first report of large anatase single-crystal cubes with predominant {001} and {010} facets via a microwave-assisted hydrothermal process. To demonstrate the applicability of such single crystal cubes, photocatalytic activity was investigated by liquid phase photocatalytic degradation of Rhodamine B (RhB) and gas phase photocatalytic oxidation of nitric oxide (NO). The obtained TiO_2 cubes were found to exhibit remarkable photocatalytic performance owing to the single-crystal nature and the high exposure of reactive crystal facets as well as fast electron transfer between two different facets.

Experimental details

Synthesis of {010} dominated Anatase TiO_2 (C010-F): In a typical synthesis, titanium tetrachloride (ACROS) aqueous solution (denoted as solution A) was prepared by dissolving 5.0 mL titanium tetrachloride in 15 mL of D. I. water which under the assisted of liquid nitrogen. Then 2 mL of ionic liquid 1-methyl-imidazolium tetrafluoroborate, synthesized according to literature,[34] was added to the titanium tetrachloride aqueous solution containing 48 mL H_2O, 0.2 g SBDS, and 2 mL of solution A. The mixture was sealed in a Teflon-lined-walled digestion vessel. After treated at a controllable temperature of 150 ^oC for 90 min using a microwave digestion system (Ethos TC, Milestone), the vessel was then cooled down to room temperature. The samples are washed with deionized water and absolute ethanol, and dried in a vacuum at 80 ^oC for 4 h. Sample C010 was obtained by the thermal treatment of C010-F at 600 ^oC for 2 h in air.

Synthesis of {001} exposed anatase TiO_2 (D001-F): {001} exposed anatase TiO_2 were prepared by a method previously published by our group.[30] Briefly, 0.04 mol/L titanium tetrafluoride (ACROS) aqueous solution was prepared by dissolving 1.24 g of titanium tetrafluoride in 250.0 mL of D.I. water which contains 0.2 mL of hydrochloric acid (37%, (MERCK)). Then 0.5 mL of ionic liquid 1-methyl-imidazolium tetrafluoroborate was added to 30.0 mL of 0.04 mol/L titanium tetrafluoride aqueous solution while stirring. The mixture was sealed in a Teflon-lined-walled digestion vessel. After treatment at a controllable temperature of 210 ^oC for 90 min using a microwave digestion system (Ethos TC, Milestone), the vessel was then cooled down to room temperature. The samples are washed with deionized water and absolute ethanol, and dried in a vacuum at 80 ^oC for 4 h. Sample D001 was obtained by the thermal treatment of D001-F at 600 ^oC for 2 h in air.

Materials Characterization

The crystallographic information of the samples were determined by X-ray diffraction (XRD, D/MAX-2000 with Cu $K\alpha_1$ irradiation), The morphology of the products were investigated by scanning electron microscopy (SEM, JEOL JSM-6380LV) and transmission electronic micrograph (TEM, JEM-2010, operated at 200 kV), The surface electronic states were analyzed by X-ray photoelectrons pectroscopy (XPS, Perkin-Elmer PHI 5000).

Activity test.

The liquid phase photocatalytic degradation of Rhodamine B (RhB) was used as a probe to evaluate the catalytic performance of the TiO_2 samples which was photocatalytically carried out at 30 °C in a self-designed 100 mL reactor containing 0.15 g catalyst and 50 mL RhB aqueous solution (10 ppm/L). Four 8 W lamps with characteristic wavelengths of 365 nm were used as the UV light source which were placed at 5 cm around the solution. The suspensions were stirred for 30 min in the dark in order to establish adsorption/desorption equilibrium between dye and the photocatalyst before illumination. At regular intervals, the catalyst was separated from the solution and the RhB concentration left in the solution was analyzed by a UV spectrophotometer (UV 7504/PC) at its characteristic wavelength (λ = 553 nm). The photocatalytic activities of the TiO_2 samples also been evaluated by the photocatalytic hydroxylation of terephthalic acid, which is always regarded as an indirection of hydroxyl radicals. Simply, 0.050 g catalyst added to 100 mL reactor containing 50 mL of 5 mM terephtaalic acid (TA) and 10 mM NaOH solution. The procedure and conditons were as same as the photocatalytic degradation of RhB. The hydroxyl radical formation at different irradiation times has been detected by measuring the fluorescence intensity at 426 nm of 2-hydroxyterephthalic acid (TAOH), which produced by the reaction of TA with hydroxyl radicals in basic solution under UV light irradiation.

The photocatalytic oxidation of NO gas was carried out in air at ambient temperature in a continuous flow rector. The volume of the rectangular reactor, which was made of stainless steel and covered with saint-Glass was 4.5 L (10*30*15 cm (h*l*w)). Eight UV-A fluorescent lamps (TL 8W) were used as the ultraviolet light source. The weight of the photocatalysts used for each experiment was kept at 0.2 g. The initial concentration of NO was diluted to about 500 ppb with an air stream supplied by a zero air generator. After the adsorption-desorption equilibrium among water vapour gases and

photocatalyst was achieved, the lamp was turned on. The concentration of NO was continuously measured by using a chemiluminescence NO analyzer (Thermo Environmental Instruments Inc. Model 42c). The NO removal rate (%) was calculated based on the following equation: NO removal rate (%) = $([NO]_{in}-[NO]_{out})/[NO]_{in}*100\%$

Results and discussion

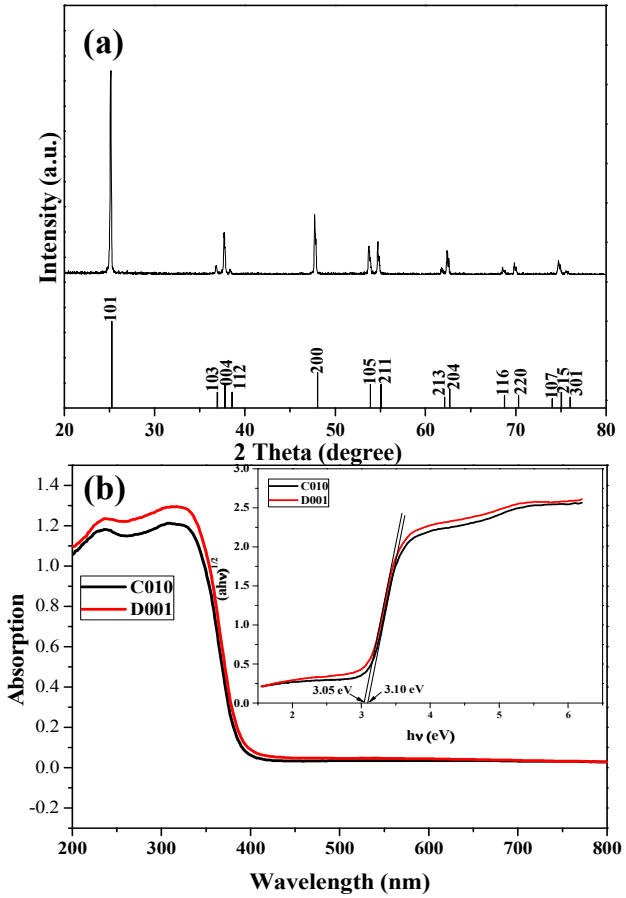

Fig. 1 (a) XRD pattern of the as-prepared TiO_2 single-crystal cubes, (b) UV-visible absorption spectrum, the inset is plots of $(ah\nu)^{1/2}$ versus photo energy (*a* represents the absorption coefficient).

X-ray diffraction (XRD) was used to characterize the phase structure and crystalline size of the sample. Figure 1a shows the XRD pattern of the as-prepared sample synthesized at 150 °C under microwave irradiation for 90 min. The diffraction pattern in Figure 1a shows that all peaks in the pattern can be assigned to the diffraction of (101), (103), (004), (112), (200), (105), (211), (213), (204), (116), (220), (107), (215), and (301) planes, clearly indicating that the sample is a pure anatase phase (tetragonal, I41/amd, JCPDS21-1272).[35] The narrow peak of the (101) with intense reflection suggests a high crystallinity of the sample. The UV-visible absorption spectra (Figure 1b) demonstrate that the absorption edge of D001 has a slight red-shift with respect to the C010 samples. The differences in absorption edge wavelength for the TiO_2 samples clearly indicate an increase in the band gap of cubic TiO_2. The band gap energies were calculated from $(ah\nu)^{1/2}$ versus photon energy plots (Figure 1b inset) to be 3.05 and 3.10 eV for D001 and C010, respectively.

Figure.2a shows the field-emission scanning electron microscopy (FE-SEM) images of the TiO_2 single-crystal cubes. The synthesized anatase single crystals have a size of around 400 nm as calculated from 50 cubes randomly selected from the FESEM images. The angle between top surfaces and lateral surface is nearly 90°, suggesting that the cube exhibits very little {101} facet. As we know, both {001} facets and {010} facets have 100 % Ti_{5c} (five-coordinate) atoms as showed in Figure 2e and Figure 2f. According to the crystal symmetry, the formation of cubic anatase TiO_2 with two top {001} facets and four lateral facets would be favored while the facets were stabilized by certain capping agents. Figure 2c, d show the bright field transmission electron microscopy (TEM) images of two different cubic anatase single crystal together with the corresponding selected area electron diffraction pattern (SAED). On the basis of SAED analysis, these cubes were consistently found to be single-crystalline. The sharp diffraction spots (Figure. 2c inset) can be ascribed to the [001] zone axis of the tetragonal anatase TiO_2 crystal. Furthermore, Figure. 2d inset shows the SAED pattern recorded along the [010] axis of the sample displaying the {002} and {101} facets with interfacial angle of 68.27°. On the basis of the above analysis, these cubes grew along the [001] direction with four {010} lateral facets and two {001} top facets.

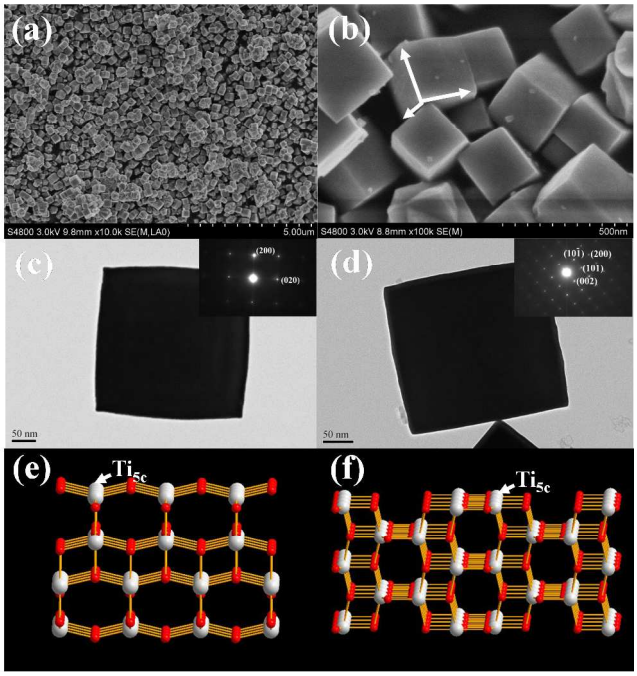

Fig. 2 low (a) and high (b) resolution FESEM images of the cubic anatase. (c, d) TEM images of two representative cubes, the insets are the corresponding SAED patterns. (e, f) schematic of atomic structure of {001} and {010} facets; grey Ti^{4+}, red O^{2-}.

It was demonstrated that the formation of Ti-F bonds changed the surface Ti_{5c} atoms to Ti_{6c}, which can significantly lower the energy of the {001} facets.[29] First-principles calculations also indicate that fluorine ions can greatly reduce the surface energy of {001} facets, making them more stable than the {101} facets and {010} facets. The anion of the ionic liquid used in this work is $[BF_4]^-$ with four

fluorine atoms in one molecule. The bulky $[BF_4]^-$ groups protect and stabilize the {001} facets[30]. The chemical state of fluorine as Ti-F species is evidenced by the F_{1s} XPS (Figure. S1), which shows a binding energy of 684.3 eV assignable to covalently-bound F species.[19] It is notable that a large number of anatase cubic aggregates with exposing a low percentage of {010} facet appeared in the absence of SDBS as displayed in Figure S2a. This result confirms that the SDBS surfactant is able to stabilize the {010} facets of anatase single crystal under the assistance of ionic liquid. To understand the exact role of SDBS in stabilizing the {010} facet of anatase, a series of experiments were carried out. Figure S2b and Figure S2c show the anatase TiO_2 obtained by using sodium dodecyl sulfonate (SDS) or hexadecyl trimethyl ammonium bromide (CTAB) as the surfactant under the identical conditions, respectively. Irregular TiO_2 crystals aggregates with exposing a large percentage of top {001} facets and a low percentage of lateral {010} facets were observed. On the basis of the above observation, the SDBS could be preferentially absorbed on the {010} facets to stabilize the {010} facets. It is worth mentioning that SDBS as an anionic surfactant is a member of the linear alkylbenzenesulfonates. This dodecyl chain is coordinated with the 4-position of the benzenesulfonate group. Generally, when SDBS are adsorbed on the surface of solid materials, there may exist the electrostatic interaction between cationic group and sulfonate anion as well as π–π stacking between aromatic rings.[36,37] Given that the typical distance between the adjacent unsaturated Ti atoms are about 0.304 nm and 0.378 nm as shown in Figure S3. This distance is consistent with that of mutual π–π stacking between aromatic rings.[37] Moreover, the anatase {010} plane is relatively flat. Considering those factors, we hypothesize that SDBS can be allowed to perpendicularly anchor onto {010} plane to form relatively tight coverage layer through electrostatic interaction between Ti_{5c} atoms and sulfonate anion accompanied with π–π stacking between aromatic rings as illustrated in Figure S4. This proposed mechanism is reasonable to explain the experimental phenomenon that the crystals aggregates with exposing a large percentage of top {001} facets and a low percentage of lateral {010} facets appeared by using SDS surfactant without aromatic ring and cationic surfactant CTAB. Therefore, both the ionic liquid and SDBS are very vital for the preferred growth of the {001} facets and {010} facets.

In general, the photocatalytic activity of catalyst is definitely affected by surface atomic structure and the percentage of exposed reactive crystal facets. These anatase TiO_2 single crystals cubes are expected to have higher reactivity due to the large percentage of {001} facets and {010} facets compared with crystals having normal majority {101} facets.[12] The sample D001-F with {101} and {001} facets dominated anatase acts as the standard to compare with C010-F. Figure S5 shows the results of XRD pattern and morphology of the as prepared D001-F. It can be observed that the well-faceted truncated octahedral has two square surfaces and the other eight isosceles assignable to {001} and {101} facet.[30] Figure 3 shows the fluorescence signal intensity of TAOH at λ= 426 nm of the samples, which was produced by the reaction of TA with hydroxyl radicals formed over TiO_2 under UV light irradiation in basic solution. The linear relationships between fluorescence intensity and irradiation time are found for all samples, as shown in the inset of Figure 3, both C010-F and D001-F exhibit low fluorescence intensity because of the surface fluorine changing the surface Ti_{5c} to Ti_{6c} which hinders the catalytic performance. The fluorinated surfaces can be cleaned by heat treatment at 600 °C for 2 h.[15] No fluorine species was detected by X-ray photoelectron spectrum (Figure S1). After removing the surface fluorine, the fluorescence signal intensity increase dramatically, indicating a significantly enhanced photocatalytic activity after removing the surface fluorine as expected. The concentration of ·OH generated from clean cubic anatase is much higher than that of decahedral anatase, demonstrating substantially improved photoreactivity of cubic anatase composed from active {001} and {010} facets. Moreover, the linear relationship between fluorescence intensity and irradiation time (Figure 3 inset) confirms the stability of those anatase cubes. This result is consistent with the recently reported higher photoreactivity of anatase TiO_2 mostly composed from {010} and {001} facets compared with the {001} and {101} facets dominated single crystal TiO_2 anatase.[19,27]

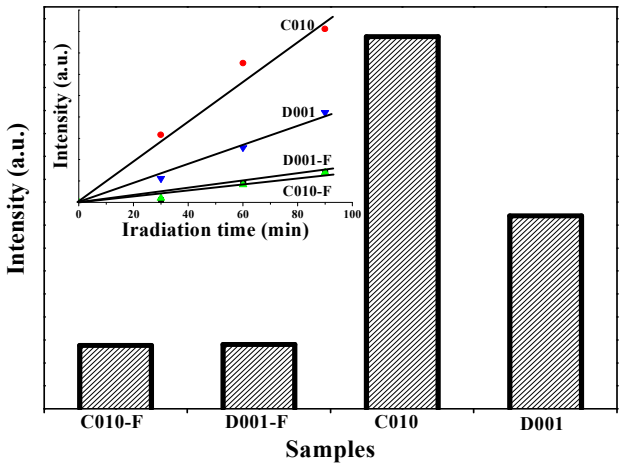

Fig. 3 Fluorescence signal intensity of anatase TiO_2 in terephthalic acid solution containing 10 mM NaOH at different UV light irradiation time. Inset is the time dependences of fluorescence intensity at λ= 426 nm over different samples.

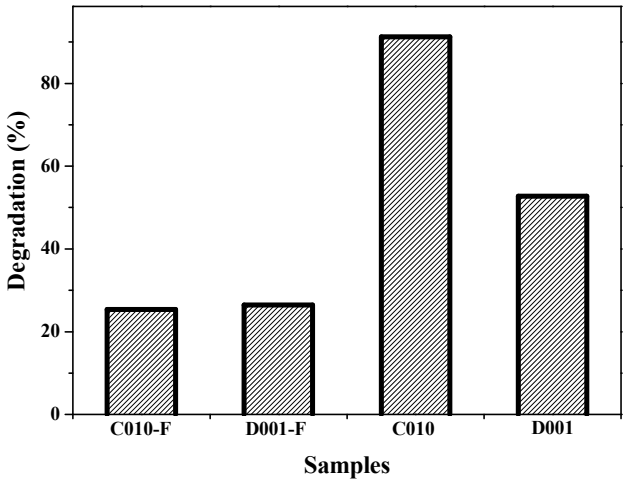

Fig. 4 The degradation yield of RhB under UV light at 90 min.

To further investigate the photoreactivity of the single crystal cubic anatase TiO_2. The anatase TiO_2 single crystals cubes were examined in photodegradation of RhB dye under UV light irradiation. As shown in the Figure 4, after removing the surface fluorine from D001-F and C010-F, the activity of photocatalytic oxidation of RhB greatly improved. Sample C010 showed the highest activity than others. The possible reason for the significantly enhanced activity on cubic anatase might be attributed to the following reason: (1) both {010} facets and {001} facets on cubic TiO_2 have the 100 % unsaturated surface Ti_{5c} atoms compared with {101} facets with 50 %. Therefore cubic anatase has higher density of unsaturated surface Ti_{5c} atoms than that of decahedral anatase, leading to efficient ·OH generation as evidenced by fluorescence test; (2) theory calculation as shown in figure S6 suggests that {010} facets have a large band gap than that of {001} facets. This result agrees well with the earlier study on TiO_2 surface band structure[19] together with the results of UV-visible spectra as shown in Figure 1b. Consequently, the photo-electrons generated from {010} facets incline to migrate to {001} facets and promote the separation of electrons and holes across the interface of the two surfaces. The more strongly reducing electron in the conduction band can be efficiently consumed by oxygen from air and thus results in the formation of superoxide radical. The superoxide radical can further react with RhB. Moreover, the efficient consumption of excited electrons can simultaneously promote the generation of holes in photocatalytic oxidation reactions; (3) the photo-exited electron on {010} facets can be transferred to {001} facets due to the higher position of conduction band compared with that of {001} facets, inhibiting the charge recombination.[12,19] In order to further demonstrate that the reasons for suppression of charge recombination of cubic TiO_2, the photoluminescence spectroscopy spectra of the sample C010 and D001were investigated and shown in figure S7. The peak around 560 nm can be assigned to the light absorption coefficient. The low peak intensity observed for the C010 clearly indicates the efficient charge separation.[38]

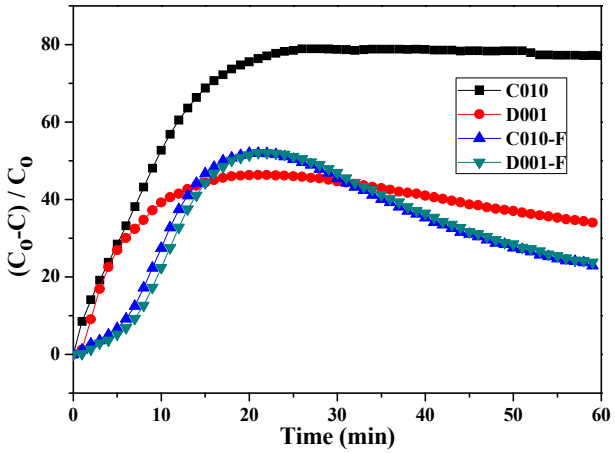

Fig. 5 Reaction profiles of photocatalytic NO oxidation of sample.

The rapid increase of NO released from continuous consumption of fossil fuels are becoming more and more urgent due to its hazardous effects on environment.[39,40] Many approaches have been devoted to gas-phase photocatalytic NO oxidation by using semiconductor photocatalysts owing to the advantages of green and easy operation under mild conditions.[30,41] The synthesized cubic anatase were further employed for photocatalytic NO oxidation. Our preliminary tests demonstrated that no significant decrease in NO content was observed in the absence of either light irradiation or photocatalyst, suggesting that the NO oxidation was mainly driven by photocatalysis. As shown in figure 5, both C010-F and D001-F samples exhibited poor activity for photocatalytic NO oxidation because the surface fluorine hinders the catalytic performance. After the removal of fluorine species by thermal treatment, C010 sample exhibited much higher NO removal rate than that of D001 sample under UV irradiation. On the one hand, C010 samples are more reactive for ·OH formation than D001 samples because of the density of unsaturated surface Ti_{5c} atoms which greatly affect the absorbability of dissociative water. Similar in the aqueous reaction, the reactive species of ·OH and the $\cdot O_2^-$, which are produce by oxidation of H_2O with photo-induced hole and reduction of O_2 with photo-excited electron, respectively, are formed more easily on {001} and {010} facets than that of {101} facets evidenced by Figure 3.[41] One the other hand, the morphology of cubic anatase contributed to the fast electron transfer because the photo-electron generated from {010} facet incline to migrate to {001} facet due to the higher conduction band position, thereby reducing photoelectron-hole recombination rate. It is noteworthy that the removal efficiency of D001 sample rapidly decreased after 20 min of reaction while the removal efficiency of sample C010 showed no appreciable lost in activity. In addition, the stability of the C010 was also investigated by recycling the photo-oxidation of NO under the same conditions as displayed in Figure S8. The results reveal that the cubic anatase TiO_2 shows excellent durability and can be used repeatedly 3 times without significant loss in activity, further suggesting the high stability of cubic anatase TiO_2.

It is well-known that the thermal stability is still a bottleneck for the practical applications of anatase TiO_2. Generally, the irreversible transformation from anatase to thermodynamically stable rutile usually occurs at a temperature of 500 °C.[35] Many approaches have been developed to increase the crystalline phase stability of TiO_2 crystals.[42] The crystalline phase stability of as-prepared cubic anatase TiO_2 was investigated by the thermal treatment of sample at different temperatures for 1 h in air. Figure S9 shown the XRD patterns of the calcined cubes. It should be noticed that the cubic anatase showed extremely high crystalline phase stability, remaining the pure anatase phase even after being calcined at 800 °C in air. Such a greatly enhanced thermal stability could be attributed to the single-crystal nature. These stable anatase TiO_2 single crystals are useful in high temperature catalysis or photoelectronic applications, such as thermal catalysis, sensors, and electronic devices.

Conclusions

In conclusion, uniform, well-defined, single crystal cubic anatase TiO_2 with predominately exposed higher-energy {010} facets and {001} facets, remarkable crystalline phase-stability, excellent enhanced photocatalytic activity were synthesized via a simple microwave-assisted process. It has been demonstrated that both ionic

liquid and SDBS played vital roles in stabilizing {001} and {010} facets through Ti-F bonds and promoting the growth of {010} facets through electrostatic interaction between Ti_{5c} atoms and sulfonate anion accompanied with π–π stacking between aromatic rings. The synthesized cubic TiO_2 showed remarkably enhanced photocatalytic activity owing the surface exposed active {001} and {010} facets, as well as unsaturated surface Ti_{5c} atoms. The synthesis methodology explored in this study is energy-saving and cost-effective, which can be developed into a general way to fabricate other metal oxide crystals on a large scale.

Acknowledgements

This work was supported by NSFC (21477079, 21207090, 21237003, 21261140333), Shanghai Government (12PJ1406800, 13YZ054, 14ZR1430900), PCSIRT (IRT1269), the doctoral program of higher education (20123127120009), the scheme administrated by Shanghai Normal University (DXL122 and S30406), the strategic China-Japan research cooperative program 2012 from JST. A part of this work was also performed under a management of "Elements Strategy Initiative for Catalysts&Batteries (ESICB)" supported by MEXT.

Notes and references

[a] Education Ministry Key Lab of Resource Chemistry and Shanghai Key Laboratory of Rare Earth Functional Materials, department of chemistry, Shanghai Normal University, Shanghai, 200234, China.
E-mail: dqzhang@shnu.edu.cn; (FAX) 86-21-6432-2272
[b] Division of Materials and Manufacturing Science, Graduate School of Engineering, Osaka University, 2-1 Yamadaoka, Suita, Osaka 565-0871, Japan.
E-mail: yamashita@mat.eng.osaka-u.ac.jp; (FAX) 06-6879-7457
[c] Unit of Elements Strategy Initiative for Catalysts & Batteries Kyoto University, ESICB, Kyoto University, Japan.
Author Contributions: † M. Wen and P. Liu. contributed equally.
Electronic Supplementary Information (ESI) available: [details of any supplementary information available should be included here]. See DOI: 10.1039/c000000x/

1 M. R. Hoffmann, S. T. Martin, W. Choi and D. W. Bahnemann, *Chem. Rev*., 1995, **95,** 69-96.
2 A. Tanaka, K. Hashimoto and H. Kominami, *J. Am. Chem. Soc.,* 2012, **134,** 14526-14533.
3 A. Tanaka, K. Hashimoto and H. Kominami, *J. Am. Chem. Soc.,* 2014, **136,** 586-589.
4 T. Kamegawa, S. Matsuura, H. Seto and H. Yamashita, *Angew. Chem. Int. Ed.,* 2013, **52**, 916-919.
5 N. Murakami, S. Katayama, M. Nakamura, T. Tsubota and T. Ohno, *J. Phys. Chem. C.,* 2011, **115,** 419-424.
6 M. Liu, H. She and S. Cheng, *J. Am. Chem. Soc.,* 2009, **131,** 3998-4005.
7 W. I. Lee, Y. Bae and A. J. Bard, *J. Am. Chem. Soc.,* 2004, **126,** 8358-8359.
8 T. Fröschl, U. Hormann, P. Kubiak, G. Kucerova, M. Pfanzelt, C. K. Weiss, R. J. Behm, N. Husing, U. Kaiser, K. Landfester and M. Wohlfahrt-Mehrens, *Chem. Soc. Rev*., 2012, **41,** 5313-5360.
9 S. Banerjee, S. C. Pillai, P. Falaras, K. E. O'Shea, J. A. Byrne and D. Dionysiou, *J. Phys. Chem. Lett.,* 2014, **5,** 2543-2554.
10 H. Fang, Y. Gao, G. Li, J. An, P. Wong, H. Fu, S. Yao, X. Nie and T. An, *Environ. Sci. Technol.,* 2013, **47,** 2704-2712.
11 H. Cheng, T. Kamegawa, K. Mori and H. Yamashita, *Angew. Chem. Int. Ed.,* 2014, **53,** 1-6.
12 G. Liu, J. C. Yu, G. Q. Lu and H. Cheng, *Chem. Commun*., 2011, **47,** 6763-6783.
13 H. B. Jiang, Q. Cuan, C. Z. Wen, J. Xing, D. Wu, X. Q. Gong, C. Li and H. Yang, *Angew. Chem. In. Ed*., 2011, **50**, 3794-3768.
14 B. Wu, C. Guo, N. Zheng, Z. Xie and G. D. Stuchy, *J. Am. Chem. Soc.*, 2008, **130**, 17563-17567.
15 C. Wang, X. Zhang and Y. Liu, *Nanoscale*, 2014, **6**, 5329-5337.
16 J. Pan, X. Wu, L. Wang, G. Liu, G. Q. Lu and H. Cheng, *Chem. Commun*., 2011, **47**, 8361-8363.
17 D. Zhang, G. Li, H. X. Yang and J. C. Yu, *Chem. Commun*., 2009, **29**, 4381-4383.
18 D. Wang, P. Kanhere, M. Li, Q. Tay, X. Tang, Y. Huang, T. C. Sum, N. Mathews, T. Sritharan and Z. Chen, *J. Phys. Chem. C*., 2013, **117**, 22894-22902.
19 J. Pan, G. Liu, G. Q. Liu and H. Cheng, *Angew. Chem. In. Ed*., 2011, **50**, 2133-2137.
20 H. Lin, L. Ding, Z. Pei, Y. Zhou, J. Long, W. Deng, X. Wang, *Appl. Catal. B: Environ*., 2014, **160-161**, 98-105.
21 J. Jiang, K. Zhao, X. Xiao and L. Zhang, *J. Am. Chem. Soc*., 2012, **134**, 4473-4476.
22 J. Yu, J. Low, W. Xiao, P. Zhou and M. Jaroniec, *J. Am. Chem. Soc*., 2014, **136**, 8839-8842.
23 A. Selloni, *Nat. Mater.*, 2008, **7**, 613.
24 Y. Jun, M. F. Casula, J. Sim, S. Y. Kim, J. Cheon and A. P. Alivisatos, *J. Am. Chem. Soc*., 2003, **125**, 15981-15985.
25 X. Gong and A. Selloni, *J. Phys. Chem. B*., 2005, **42**, 19560-19562.
26 Z. Lai, F. Peng, Y. Wang, H. Wang, H. Yu, P. Liu and H. Zhao, *J. Mater. Chem*., 2012, **22**, 23906-23912.
27 X. Zhao, W. Jin, J. Cai, J. Ye, Z. Li, Y. Ma, J. Xie and L. Qi, *Adv. Funct. Mater.*, 2011, **21**, 3554-3563.
28 D. Zhang, R. Wang, M. Wen, D. Weng, X. Cui, J. Sun, H. Li and Y. Lu, *J. Am. Chem. Soc.,* 2012, **134**, 14283-14286.
29 H. G. Yang, C. H. Sun, S. Z. Qiao, J. Zou, G. Liu, S. C. Smith, H. M. Cheng and G. Q. Lu, *Nature*, 2008, **453**, 638-641.
30 D. Zhang, G. Li, H. Wang, K. M. Chan and J. C. Yu, *Crys. Growth Des.*, 2010, **10**, 1130-1137.
31 C. K. Nguyen, H. G. Cha and Y. S. Kang, *Crys. Growth Des.*, 2010, **11**, 3947-3953.
32 J. Zhang, L. Qian, W. Fu, J. Xi and Z. J, *J. Am. Ceram. Soc.*, 2014, **97**, 2615-2622.
33 X. Han, Q, Kuang, M. Jin, Z. Xie and L. Zheng, *J. Am. Chem. Soc.,* 2009, **131**, 3152-3153.

34 J. D. Holbrey and K. R. Seddon, *J. Chem. Soc., Dalton Trans.,* 1999, 2133-2139.
35 D. Zhang, M. Wen, P. Zhang, J. Zhu, G. Li and H. Li, *Langmuir,* 2012, **28**, 4543-4547.
36 J. J. Brege, C. E. Hamilton, C. A. Crouse and A. R. Barron, *Nano. Lett.*, 2009, **9**, 2239-2242.
37 J. Zhu, J. Wang, F. Lv, S. Xiao, C. Nuckolls and H. Li, J. Am. Chem. Soc, *J. Am. Chem. Soc.*, 2013, **135**, 4719-4721.
38 J. Zhu, J. Ren, Y Huo, Z. Bian and H. Li, *J. Phys. Chem. C.,* 2007, **111**, 18965-18969.
39 A. Fritz and V. Pitchon, *Appl. Catal. B: Environ.*, 1997, **13**, 1-25.
40 H. Bosch and F. Janssen, *Catal. Today*, 1988, **2**, 369-531.
41 D. Zhang, M. Wen, S. Zhang, P. Liu, W. Zhu, G. Li and H. Li, *Appl. Catal. B: Environ.*, 2014, **147**, 610-616.
42 C. Kang, L. Jing, T. Guo, H. Cui, J. Zhou and H. Fu, *J. Phys. Chem. C.,* 2009, **113**, 1006-1013.